SCIENCE CHINA
Technological Sciences

•Article•

July 2021 Vol.64 No.7: 1513–1527
https://doi.org/10.1007/s11431-020-1788-4

An improved modeling of precipitation phase and snow in the Lancang River Basin in Southwest China

HAN ZhongYing[1], LONG Di[1*], HAN PengFei[1], HUANG Qi[1], DU MingDa[1] & HOU AiZhong[2]

[1] *State Key Laboratory of Hydroscience and Engineering, Department of Hydraulic Engineering, Tsinghua University, Beijing 100084, China;*
[2] *Hydrological Forecast Center, Ministry of Water Resources of the People's Republic of China, Beijing 100053, China*

Received April 12, 2020; accepted February 5, 2021; published online May 31, 2021

Precipitation phase (e.g., rainfall and snowfall) and snow (e.g., snowpack and snowmelt runoff) in high-mountain regions may largely affect runoff generation, which is critical to water supply, hydropower generation, agricultural irrigation, and ecosystems downstream. Accurately modeling precipitation phase and snow is therefore fundamental to developing a better understanding of hydrological processes for high-mountain regions and their lower reaches. The Lancang River (LR, or the Upper Mekong River) in China, among the most important transboundary rivers originating from the Tibetan Plateau, features active dam construction and complex water resources allocation of various stakeholders in Southeast Asian countries under climate change. This study aims to improve precipitation phase and snow modeling for the LR basin with a hydrological model and multisource remotely sensed data. Results show that joint use of the Moderate Resolution Imaging Spectroradiometer (MODIS) land surface temperature product with high spatial resolution (1 km×1 km) and an air temperature product can more precisely distinguish precipitation phase than air and wet-bulb temperature products in the LR basin. Snowfall and snowmelt were found to be controlled primarily by rainfall and snowfall temperature thresholds in snow modeling. The rainfall and snowfall temperature thresholds derived from the hydrological model through calibration with remotely sensed snowpack at basin scales were considerably lower than those derived from *in situ* observations. Rainfall and snowfall temperature thresholds derived from *in situ* observations could lead to the overestimation of snowmelt runoff due mostly to the lack of representation of point-based measurements at basin scales. This study serves as a basis for better modeling and predicting snow for the LR basin and potentially other similar basins globally.

distributed hydrological model, snowfall, snow water equivalent, snowmelt, Lancang River Basin

Citation: Han Z Y, Long D, Han P F, et al. An improved modeling of precipitation phase and snow in the Lancang River Basin in Southwest China. Sci China Tech Sci, 2021, 64: 1513–1527, https://doi.org/10.1007/s11431-020-1788-4

1 Introduction

Mountains provide freshwater resources for downstream human activities. The Intergovernmental Panel on Climate Change indicates that the mean annual temperature for High Asia will increase from 1 to 6°C by 2100 [1]. Runoff from the Tibetan Plateau (TP), known as Asia's water towers, tends to be quite sensitive to climate change as a result of snow and glacier melting [2,3]. Changes in snow (e.g., snowpack and snowmelt runoff) may have a long-term impact on the sustainable development of downstream areas [4]. Accurately simulating snow melting processes for river basins on the TP is therefore particularly important for downstream water supply, hydropower operation, and flood forecasting, and is fundamental for reliable prediction of changes in runoff in the future.

Some studies have investigated the impact of climate change on water availability in the Mekong River basin (MRB), with its upper reaches within China termed the Lancang River (LR) [5–8]. These studies used output from a

*Corresponding author (email: dlong@tsinghua.edu.cn)

few number of general circulation models to represent future climate scenarios, and then examined the impact of climate change on runoff, water and wetland resources, and extreme events. The studies mentioned above focused on hydrological processes for the MRB, but few studies focused on the LR and its upper reaches (ULR) [9,10].

Successful modeling and prediction of cryospheric processes in high-mountain regions need reliable observational data, a suited hydrological model, and reasonable estimation of model parameters [11]. The LR originates at over 5100 m above the sea level on the TP where *in situ* observations are extremely sparse. Satellite remote sensing is valuable in deriving hydrological components at varying spatiotemporal scales, without being largely affected by complex climate systems and terrain [12–19]. Precipitation is the primary forcing in hydrological modeling. The Global Satellite Mapping of Precipitation (GSMaP) product as one of remote sensing precipitation products has been found suited for basin-scale hydrological modeling in warm regions [20–22].

Hydrological models with a snow and glacier melt module are fundamental tools for simulating and predicting cryospheric processes in high-mountain regions. Melt runoff models generally fall into two categories: energy balance models and temperature-index models. Temperature-index models are more readily applicable to basin scales with accessible temperature data, and may have better model performance and computational simplicity [23].

Identifying surface precipitation phase is required in both energy balance-based and temperature-index models to determine the hydrological response to precipitation events, because rainfall will be treated differently from snowfall in hydrological modeling. Current ways of observing precipitation phase include direct observations with observers identifying the phase of falling precipitation, ground-based remote sensing observations, and spaceborne remote sensing observations [24]. Direct observations are valuable but subject to the difficulty of identifying mixed-phase events and the lack of observations in remote areas and/or during low-light conditions. Ground-based remote sensing observations are difficult to apply to complex terrain. Spaceborne remote sensing observations using passive microwave (PMW) sensors are subject to coarse spatial resolutions whereas observations using active microwave sensors remain largely unverified [25,26]. No high-quality gridded precipitation-phase observations are currently available as forcing data sets for hydrological modeling, so accurate phase identification methods are urgently needed.

Most state-of-the-art models rely on simple empirical relationships to predict precipitation phase. For example, most hydrological models use temperature-based thresholds that do not consider near-surface humidity [24]. Furthermore, most models, e.g., Snowmelt Runoff Model (SRM), Hydrologiska Byråns Vattenbalansavdelning (HBV) model, Snow Accumulation and Ablation Model (Snow-17), Noah, and Variable Infiltration Capacity (VIC) model, use a single static temperature threshold, which may result in lower accuracy than multiple temperature methods [27–30]. Marks et al. [31] evaluated methods for distinguishing precipitation phase in mountain basins and found that precipitation phase in mountain basins is linked to during-storm humidity. Ding et al. [32] investigated the relationship between precipitation types and meteorological variables and found that wet-bulb temperature including information on additional humidity and air pressure could be a better indicator than near-surface air temperature for distinguishing precipitation phase. To advance hydrological modeling over high-mountain cryospheric regions, reliable thresholds for distinguishing precipitation phase must be fully investigated.

Estimation of hydrological model parameters is another key issue. In general, hydrological model calibration is based on the hypothesis that a unique set of parameters ensures an optimal match between simulated and observed river discharge [33]. Use of more observed hydrological variables in model calibration may improve the performance of hydrological models [34,35]. Considering snow meltwater in high-mountain regions, snow cover area (SCA), snow depth, and snow water equivalent (SWE) can be jointly used with discharge observations in model calibration. The 500 m resolution MODIS (moderate resolution imaging spectroradiometer) snow products contain daily, gridded snow cover and albedo derived from radiance data acquired by the MODIS, which is a key instrument aboard the Terra and Aqua satellites. Most studies used the MODIS SCA products to calibrate the model and then simulated the snowmelt runoff process [2,36–38]. The MODIS SCA products are subject to cloud cover and few published studies adequately evaluated the reliability of SCA products and simulated SCA from hydrological models. Johnson et al. [39] found that the utilization of high resolution PMW Daily EASE-Grid 2.0 Brightness Temperature ESDR data which are related to snow depth could help detect snowmelt in heterogeneous terrain accurately. Some studies used PMW remote sensing-based SWE retrievals only or both SCA and SWE to calibrate hydrological models. Debeer and Pomeroy [40] used measured SWE to simulate the contributing area of snowmelt runoff in a small alpine basin. Stigter et al. [41] assimilated both MODIS SCA products and SWE observations into a snow model to estimate snowmelt runoff. These two studies evaluated the SWE simulations, but the validation period spanned only a few months due to the limited time span of SWE observations. The ability of a hydrological model to simulate snowmelt runoff depends largely on how well the model simulates the snowmelt processes. Sensitivity analysis of parameters of snow models needs to be performed to identify the behavior of snowmelt parameters and subsequently to reduce modeling uncertainties.

This study aims to improve precipitation phase and snow modeling in the LR basin by using: (1) precipitation and temperature products with the best performance in SWE modeling, (2) appropriate rainfall and snowfall temperature thresholds to identify precipitation phase, and (3) a quality snow depth product to calibrate the snow module. A distributed hydrological model (coupled routing and excess storage, CREST) [42,43] coupled with a snow and glacier melt module [33] (termed CREST-snow model hereafter) was utilized here. Specifically, the study aims to: (1) evaluate the performance of different precipitation and temperature products in snow modeling; (2) examine the sensitivity of parameters associated with snow accumulation and melting; (3) compare the rainfall and snowfall temperature thresholds derived from the hydrological model and those derived from *in situ* observations.

2 Study area

The LR is among the largest rivers in Southwest China, located within the domain 22°05′N–33°40′N and 93°50′E–101°30′E (Figure 1). The LR flows through Qinghai, Tibet, and Yunnan Provinces with a total length of ~2140 km and a drainage area of ~142000 km^2. It originates from Zadoi County in Qinghai on the TP and serves as an important freshwater source for downstream countries (i.e., Burma, Thailand, Laos, Cambodia, and Vietnam). The terrain of the LR basin is complex, with decreasing elevations from its northwest of ~5800 m to southeast of ~600 m. Accounting for ~55% of the LR basin area, the northern part (upstream of the Changdu gauging station and Liutongjiang gauging station as shown in Figure 1, termed the Changdu basin and upper Lancang River (ULR) basin respectively hereafter) is characterized by snow mountains with elevations ranging from ~2200 to ~5600 m. Its unique geographical features and tremendous hydropower potential favor cascade hydropower development in this area [44]. Basin characteristics of each study basin are shown in Table 1.

The LR is characterized by a subhumid climate, with mean annual precipitation of ~620 mm in the ULR basin and a humid climate with mean annual precipitation of ~830 mm across the entire LR basin above the Yunjinghong gauging station based on a 7-year record (2008–2014) of the China

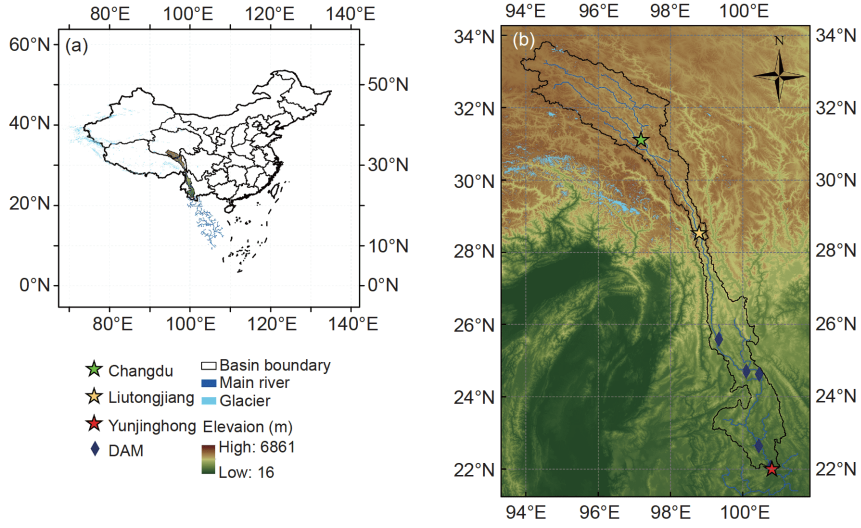

Figure 1 Location of the LR basin, three streamflow gauging stations (i.e., Changdu, Liutongjiang, and Yunjinghong from the upper, middle, to the lower reaches), dams, glacierized areas, and elevation (m). There are currently no big dams in the ULR basin, showing natural flow regimes without being largely affected by reservoir operation.

Table 1 Basin characteristics of the Changdu, ULR and LR basins

Variable	River basin		
	Changdu	ULR	LR
Location	93°E–98°E, 31°N–34°N	93°E–99°E, 28°N–34°N	93°E–102°E, 22°N–34°N
Basin area (km^2)	54228	77380	142000
Glacierized area (km^2)	131	157	160
Elevation range (m)	3240–5640	2177–5640	548–5812
Discharge gauge	Changdu	Liutongjiang	Yunjinghong
Number of meteorological stations	2	3	30

gauge-based daily precipitation analysis (CGDPA) product [45]. The climate in the LR basin is influenced strongly by both the Indian summer monsoon and westerlies, resulting in marked precipitation variability in wet and dry seasons from southeast to northwest. Furthermore, the LR exhibits strong seasonality in runoff, with 70% of the annual discharge and the highest discharge normally occurring in Aug and Sep [46].

3 Methodology

3.1 Methods

This study aims to improve snowmelt runoff modeling at three key cross-sections (Figure 1) of the LR in China. First, the snowmelt module was driven by a combination of different precipitation and temperature products to simulate SWE. A quality remote sensing snow depth product of 500 m spatial resolution which was validated by *in situ* snow depth measurements was used to calibrate the snowmelt module. Then the optimal combination of the precipitation and temperature products with the best performance in SWE modeling was determined. Second, CREST-snow model forced by the optimal precipitation and temperature products was used to model snowmelt runoff and total runoff. Third, sensitivity analysis was performed to figure out crucial parameters for snowmelt runoff modeling. Figure 2 shows the framework of this study.

3.1.1 *Snowmelt module*

A snowmelt module based on the temperature-index method was used here to simulate SWE. Daily precipitation gridded products including the rain gauge-based product (CGDPA) and satellite-based precipitation estimates (GSMaP), and daily temperature gridded products including land surface temperature (LST), near-surface air temperature (T_a), and wet-bulb temperature (T_w) were used as forcing data. SWE calculated using snow depth retrievals from PMW remote sensing and *in situ* snow density measurements from the Environmental and Ecological Science Data Center for West China (WestDC) was used to calibrate and validate the snowmelt module [33]. The snowmelt module was run from Jul 2003 to Dec 2010, with the calibration period during Jul 2003–Dec 2005 and the validation period during Jan 2006–Dec 2010. It was run under six scenarios, including different combinations of two precipitation and three temperature products in the Changdu, ULR and LR basins, respectively. Each scenario was calibrated with its individual forcing data sets.

In the snowmelt module, T_a, T_w or the arithmetic mean of LST and T_a can be used to partition total precipitation into solid or liquid phase. T_a was the most commonly used variable to distinguish precipitation phase in previous studies [9,10,47]. LST products were shown to improve the spatial

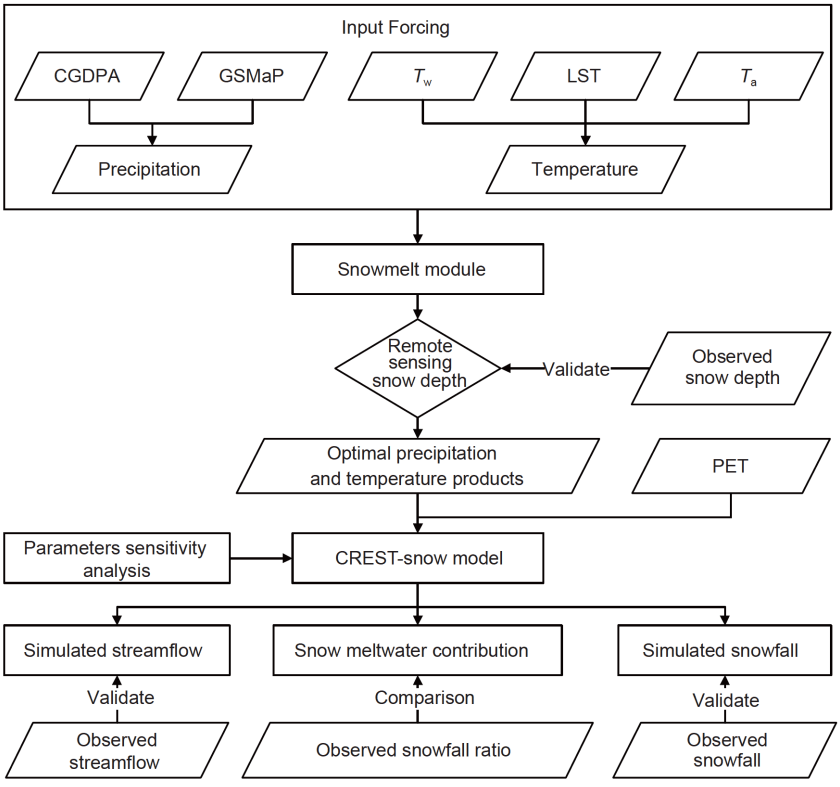

Figure 2 Flowchart of this study, including forcing and validation data sets of the snowmelt module and CREST-snow model.

pattern of simulated hydrological variables due to its high spatial resolution [33,48–50]. T_w includes information on additional humidity and air pressure than near-surface air temperature. The three types of temperature products may have their own advantages and limitations in snowfall and snowmelt modeling in our study basins. T_a observations were used to determine if the snow starts to melt. In most hydrological models, the precipitation phase is determined according to one or two air temperature thresholds, which are, however, predetermined from the literature [51] and the snowmelt temperature is often set at about 0°C [52,53]. In this study, all the parameters of the snowmelt module (the last five parameters as shown in Table 2) were determined by model calibration.

3.1.2 CREST-snow model

The CREST-snow model was updated by adding the snowmelt module [33] and a groundwater module to the CREST V2.1 model [42,43]. CREST-snow model computes infiltration and runoff using the storage capacity curve updated from the Xinanjiang hydrological model [54]. Linear reservoirs are employed to simulate sub-grid cell routing in a study basin, resulting in accurate streamflow simulations [55]. It was set up at a spatial resolution of 1 km to simulate daily streamflow including rainfall-runoff, snow and glacier meltwater at the Liutongjiang and Yungjinghong gauging stations, respectively. Daily precipitation, potential evapotranspiration (PET) and temperature gridded products were used as forcing data. Snow related parameters were calibrated first using the snowmelt module and SWE data sets as mentioned in Section 3.1.1. Other parameters were calibrated using streamflow observations. Each basin was calibrated using its individual forcing data sets. In this study, the parameters were calibrated automatically using the non-dominated sorting genetic algorithm II (NSGA-II) [56]. The major parameters that need to be calibrated for the CREST-snow model are listed in Table 2. The calibrated degree-day factors for snowmelt and icemelt are similar to the observed ones in the Himalayas in previous study, showing the reliability of these parameters in this study [57].

Daily streamflow observations at the Liutongjiang gauging station were used to calibrate and validate the model for the periods of Jul 2011–Dec 2013 and Jan 2014–Dec 2015, respectively. Daily discharge observations at the Yunjinghong gauging station which is the outlet of the LR basin were used for calibrating and validating the model for the period Jan 2004–Dec 2006 and Jan 2007–Dec 2011, respectively; data since 2012 onwards were not used for validation because the streamflow regime has been profoundly altered by reservoir operations [58].

Due to the confidentiality of streamflow observations, streamflow simulations and observations were normalized using the min-max normalization. It is a normalization strategy which linearly transforms x to $y=(x-\min)/(\max-\min)$, where "min" and "max" denote the minimum and maximum values in streamflow time series in each subfigure in the Results section. The performance of the model was evaluated using the Nash-Sutcliffe model efficiency coefficient (*NSE*), correlation coefficient (*CC*), and relative differences (*Bias*). *Bias* here is defined as the sum of the difference between simulations and observations, divided by the sum of observations. It is expressed as a fraction in the SWE simulation or a percent in the runoff simulation.

3.1.3 Sensitivity analysis of snowmelt parameters

A sensitivity analysis of snowmelt parameters was performed to identify the critical parameters in snowmelt modeling. Snowmelt-related parameters include: (1) rainfall and snowfall temperature thresholds which were used to identify precipitation phase; (2) snowmelt temperature threshold; (3) degree-day factors which stand for snowmelt rates. The CREST-snow model was run by varying one class of parameters at a time and keeping the other two classes of parameters at their default values. Then we compared the contributions of snowmelt runoff to total runoff using different parameters.

Table 2 Major parameters and their ranges in the CREST-snow model

Model parameters	Range		Optimized values		
	Min	Max	Changdu	ULR	LR
Mean water capacity, W_m (mm)	80	300	–	106.04	158.98
Exponent of the variable infiltration curve, B	0.05	1.5	–	0.86	0.61
Glacier ice melt temperature threshold, $T_{i,\mathrm{mlt}}$ (°C)	−5	5	–	0.49	0.63
Degree factor for ice melt, $d_{\mathrm{i,mlt}}$ (mm °C^{-1} d^{-1})	0	10	–	5.81	7.13
Snowmelt temperature threshold, $T_{\mathrm{s,mlt}}$ (°C)	−8	8	−5.68	−2.60	−1.71
Snowfall temperature threshold, T_s (°C)	−5	5	−2.25	−3.61	−0.32
Rainfall temperature threshold, T_r (°C)	−5	5	1.15	−0.61	2.50
Max. degree factor for snowmelt, $d_{\mathrm{s,mlt6}}$ (mm °C^{-1} d^{-1})	0	10	6.58	5.03	6.36
Min. degree factor for snowmelt, $d_{\mathrm{s,mlt12}}$ (mm °C^{-1} d^{-1})	0	5	1.41	0.56	1.19

3.1.4 Evaluation of snowfall and snowmelt runoff modeling

Snowfall observations from the China Meteorological Administration (CMA) were obtained for use in evaluating snowfall and snowmelt runoff simulations. First, time series of snowfall simulations and observations were compared. Second, rainfall and snowfall temperature thresholds derived from the snowmelt module and those from gauge observations were compared. Third, percentages of total runoff originating as snowmelt and precipitation falling as snow in the study basins were compared.

The terrain in the LR basin varies greatly (Figure 1), including plateau, mountains, canyons, and alluvial plains. The LR basin spans multiple climatic zones from north to south, including the frigid, frigid-temperate, temperate, sub-tropical, and tropical zones [59]. The amount of snowfall is relatively high in mountainous regions in the northern part of the LR basin, while it is close to zero in the southern part. There are 30 meteorological stations located within and surrounding the LR basin, with 3 located in the ULR basin. Snowfall observations at stations Nos. 56018, 56125 and 56137 located in the ULR basin were used to evaluate snowfall simulations at the grid cells where the stations are located. Several widely used statistical indicators were used to quantitatively evaluate the performance of the snowfall modeling, including the relative bias (*Bias*), root mean square error (*RMSE*) and correlation coefficient (*CC*). Probability of detection (POD), false alarm ratio (FAR), and the critical success index (CSI) were jointly used to describe the contingency of snowfall modeling. Specific formulas of the above indices can be found in Tang et al. [60].

A double temperature threshold method was used here to distinguish snowfall, rainfall, and sleet events. Precipitation with temperatures below the snowfall temperature threshold is considered as snow, while precipitation with temperatures above the rainfall temperature threshold is considered as rain. Precipitation with temperatures between these two temperature thresholds is considered sleet. To derive temperature thresholds for a station using observed data, we extracted air temperature data of all sleet events from 2003 to 2014 for the station and sorted them in descending order. Then the 5% and 95% quantiles of the air temperature data were taken as the rainfall and snowfall temperature thresholds respectively for this station. The temperature thresholds for a basin were approximated by the mean of the thresholds of all meteorological stations located within and surrounding the basin. The rainfall and snowfall temperature thresholds derived from station observations were compared with those derived from the snowmelt module through calibration with remotely sensed SWE.

In the end, contributions of snowmelt to total runoff calculated through the modeling were compared with snowfall rates based on gauge observations for the time period Jan 2004–Dec 2010 in these study basins. There was no comparison in the ULR basin because daily streamflow observations at the Liutongjiang gauging station were available only for the period of Jul 2011–Dec 2015.

3.2 Data sets

3.2.1 Precipitation and snowfall

Precipitation is the primary forcing in hydrological models for runoff and, particularly, for snowmelt modeling in this study. Since the Changdu and ULR basins are high-mountain regions with relatively sparse rain gauges, different precipitation data sets were used to develop a better understanding of how uncertainty in precipitation impacts hydrological modeling. Two precipitation products including the CGDPA and GSMaP were used to drive the hydrological model.

The CGDPA precipitation product developed by the CMA's National Meteorological Information Center (NMIC), spanning from 1955 through 2014 at a spatial resolution of 0.25°×0.25°, was generated using rainfall measurements of ~2400 national gauges and the climatological optimal interpolation algorithm [61].

Satellite-based precipitation products provide comprehensive estimation of precipitation on the global scale. GSMaP was originally sponsored by the Japan Science Technology Agency and is currently sponsored by the Japan Aerospace Exploration Agency. The objective of this project was to map global precipitation with 0.1° and 1-hour resolutions. GSMaP used the Kalman filter to update precipitation rates after propagating rain pixels along with atmospheric motion vectors [62]. The GSMaP_Gauge_RNL product using the Japanese 55-year Reanalysis was used from Jan 2003 to Feb 2014 and the GSMaP_Gauge product was used from Mar 2014 to Dec 2015.

The snowfall data set was developed using snowfall observations from ~2400 meteorological stations across Mainland China during 2003–2014. The data set was obtained from the CMA.

3.2.2 Temperature

Daily near-surface air temperature gridded products including daily maximum, minimum, and average air temperature were developed by the CMA's NMIC using data from ~2400 meteorological stations across Mainland China and the thin-plate spline method (http://cdc.nmic.cn). The data set has a spatial resolution of 0.5°×0.5°.

Atmospheric pressure and dewpoint temperature were taken from the interim European Centre for Medium-Range Weather Forecasts (ECMWF) Re-Analysis (ERA-Interim) dataset. ERA-Interim is a global atmospheric reanalysis produced by the ECMWF. An advantage of using reanalysis is that the data provide a global view that encompasses many

essential climate variables in a physically consistent framework and cover a long time period from Jan 1979 onwards. Here daily ERA-Interim pressure and dewpoint temperature estimates at a spatial resolution of 0.125°×0.125° for the period 2003–2014 were used. Relative humidity can be calculated using air temperature, dewpoint temperature, and atmospheric pressure. Bao and Zhang [63] evaluated four widely used reanalysis products including the NCEP (National Centers for Environmental Prediction)-NCAR (National Center for Atmospheric Research) reanalysis, NCEP Climate Forecast System Reanalysis (CFSR), 40-yr ECMWF Re-Analysis (ERA-40), and ERA-Interim products with sounding observations from an enhanced radiosonde network available every 6 h during the Tibetan Plateau Experiment conducted from 10 May to 9 August 1998 on the Tibetan Plateau. Results suggest that the quality of the relative humidity analysis may be highly uncertain among all variables including wind speed, surface air temperature, pressure, and relative humidity. However, the ERA-Interim has the smallest overall RMSE in relative humidity ranging without much change in magnitude throughout the vertical column. Wet-bulb temperatures can be calculated using the following two equations:

$$e_s = 6.1078 \times e^{\left(\frac{17.27\times T}{273.3+T}\right)}, \quad (1)$$

$$T_W = T - \frac{e_s \times (1-RH)}{0.000643 \times P - e_s'}, \quad (2)$$

where e_s is the saturated vapor pressure (hPa); T is the daily average near-surface air temperature (°C); T_w is the wet-bulb temperature (°C); RH is the relative humidity; P is the actual atmospheric pressure (hPa); and e_s' is the first-order derivative of eq. (1).

Meteorological stations and ground surveys are often sparse and/or irregularly distributed across complex terrain. Remotely sensed land surface temperature (LST) can be a critical source of data for snowmelt modeling [64,65]. MODIS provides good resolutions in space (500–1000 m) and time (approximately 4 observations per day) at regional scales. The LST product was reconstructed based on a multi-temporal classification and robust regression approach [66]. Based on four observations of instantaneous LST per day from the Terra and Aqua satellites, an empirical LST diurnal variation model GOT01_0 [67,68] was used to calculate daily average LST. The LST data used in this study were spatially consistent and temporally continuous, which was sufficient for snowmelt modeling.

3.2.3 *Snow water equivalent*

Global SWE products (e.g., AMSR-E SWE products) always have large uncertainties [69]. Here SWE was estimated using a snow depth product obtained from the WestDC (http://westdc.westgis.ac.cn/) [70–73]. A new spatial dynamic method was used by introducing ground emissivity and assimilating the snow cover fraction and MODIS LST to derive snow depth at a spatial resolution of 500 m during 2003–2010. In this method, ground emissivity was calculated using Advanced Microwave Scanning Radiometer-Earth Observing System brightness temperatures and MODIS LST. Additionally, the microwave emission model of layered snowpack was applied to simulate brightness temperatures with varying ground emissivity to determine the key coefficients in the snow depth retrieval algorithm [71–73]. Subsequently, the SWE was calculated as follows and it was used to calibrate the snowmelt module of the hydrological model:

$$\mathrm{SWE} = \frac{\rho_{\mathrm{snow}} \times sd}{\rho_{\mathrm{water}}} = \frac{0.1966 \times sd^{0.9063}}{\rho_{\mathrm{water}}}, \quad (3)$$

where ρ_{snow} is the snow density; sd is the PMW-based snow depth of snowpack; and ρ_{water} is the density of liquid water. The snow density was derived by Chen et al. [33].

Compared with *in situ* snow depth measurements during 23rd–30th March 2014, the bias and root-mean-square error of the new snow depth were ~1 and ~7 cm, respectively. These metrics are much lower than those of ~6 and ~10 cm using a previous product [73]. Figure 3 shows time series of snow depth observations from CMA and the new snow depth product at the grid cell where the gauge is located from West-DC. The biases (the sum of the difference between snow depth from West-DC and CMA, divided by the sum of snow depth from CMA) of the new snow depth product at these two gauges are 0.41 and −0.07, respectively. The overestimation in ground emissivity difference is the main factor causing the overestimation of snow depth [73].

3.2.4 *Other data*

PET data were obtained from the Famine Early Warning Systems Network (http://earlywarning.usgs.gov/fews). The

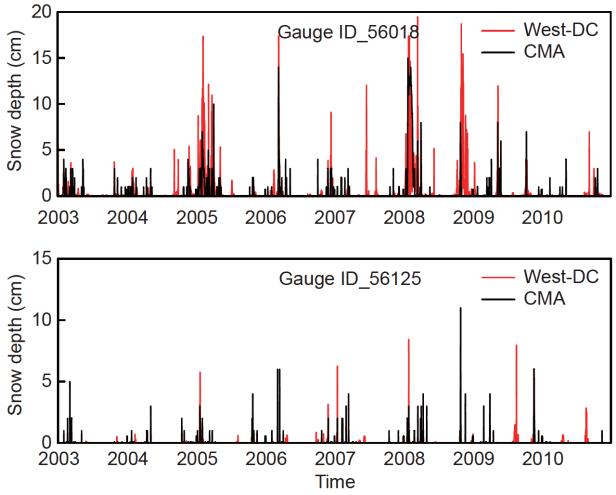

Figure 3 Comparisons of the new snow depth product (West-DC) with in situ snow measurements (CMA) at two gauges in the LR basin.

daily global PET estimate is calculated using climate variable output from global data assimilation system (GDAS) analysis fields and the Penman-Monteith equation [74]. The overall glacierized area of each study basin was extracted from the Randolph Glacier Inventory (RGI 5.0). Daily discharge data at the Liutongjiang and Yunjinghong gauging stations during May 2011–Dec 2015 and Jan 2003–Dec 2014, respectively, were obtained for warm up, calibration and validation purposes in combination with other data sets. The digital elevation model (DEM) provided by NASA's Shuttle Radar Topography Mission (SRTM) was used to delineate the basin boundary. Flow direction and flow accumulation in the CREST-snow model with a spatial resolution of 1 km × 1 km were also derived from the SRTM DEM.

4 Results

4.1 Snow water equivalent modeling

Although snow covers only ~5% of the Lancang River Basin, SWE and meltwater may have a substantial impact on the runoff, particularly during the low-flow period [75]. Input data sets and model parameters are particularly important for snowmelt modeling. Hydrological models serve as an effective tool by looking at the performance of hydrological modeling under different inputs. The performance of SWE modeling driven by the combination of two precipitation products and three temperature estimates was investigated using the snowmelt module.

A previous study suggested that hydrological modeling with an NSE>0.50 can be considered satisfactory [76]. Statistical metrics of the simulated SWE are given in Figure 4. Results of the simulated SWE for the overall period of Jul 2003–Dec 2010 suggest that the snowmelt module is able to simulate SWE well (NSE>0.5) using appropriate forcing data sets in all the Changdu, ULR and LR basins. GSMaP and LST performed best (e.g., the NSE values of 0.58, 0.58, and 0.59 during the validation period of 2006–2010 for the Changdu, ULR and LR basins) in three study areas in all combinations of precipitation and temperature estimates.

Overall, GSMaP performed better than CGDPA in all three basins with higher NSE values. The rain gauge density (the number of rain gauges per 1000 km^2) is 0.06, 0.08, and 0.2 in the Changdu, ULR and LR basins, respectively. This manifests the potential of GSMaP satellite precipitation over ungauged or poorly gauged basins, which is valuable in improving our understanding of hydrological processes over these areas.

The LST product used in this study is spatially consistent and temporally continuous. Use of LST provides tremendously valuable information at a spatial resolution of 1 km that is able to reflect temperature gradients with elevation and terrain. This is important to hydrological modeling across mountainous regions. Many studies showed that wet-bulb temperatures including additional information on humidity and air pressure could be a better indicator than near-surface air temperature for distinguishing precipitation phase [31,32,77]. However, the wet-bulb temperature data used here did not perform well in SWE modeling (e.g., the overall NSE values of 0.37 for T_w and GSMaP precipitation and 0.4 for T_a and GSMaP precipitation in the Changdu basin). The quality of the wet-bulb temperature data might be influenced by large uncertainty in relative humidity estimates calculated using the ERA-Interim product [63]. The air temperature data product used here was interpolated by *in situ* measurements that are generally sparse in this region, with very course spatial resolution of 0.5°. In conclusion, joint use of LST and air temperature data can better reflect rain-snow partitioning and, subsequently, SWE modeling in our study basins.

Time series of the simulated SWE using GSMaP and LST against the PMW-based SWE reference and corresponding

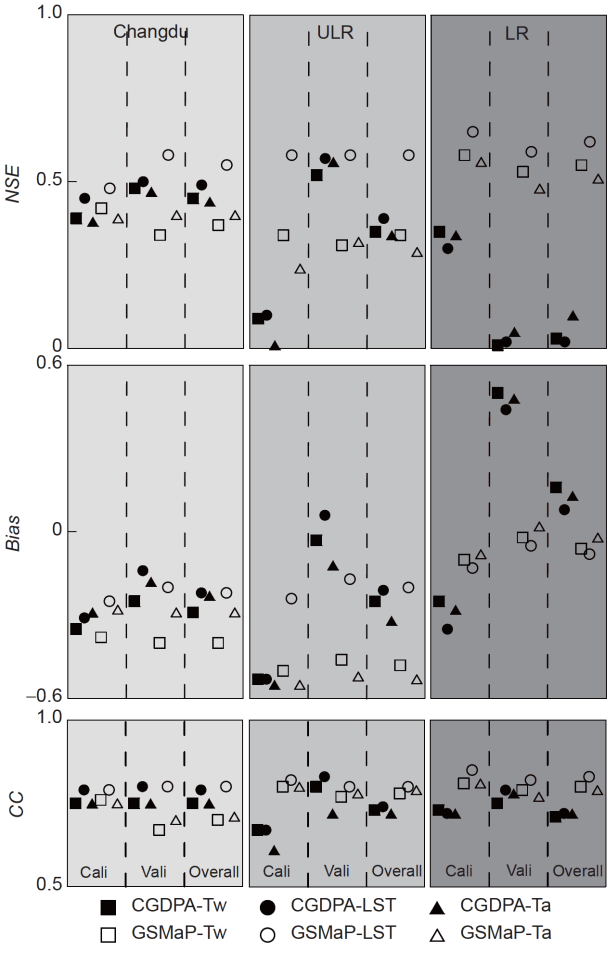

Figure 4 Statistical metrics of SWE modeling using different combinations of precipitation and temperature data sets during the calibration period (Jul 2003–Dec 2005), validation period (Jan 2006–Dec 2010), and entire study period in the Changdu, ULR and LR basins.

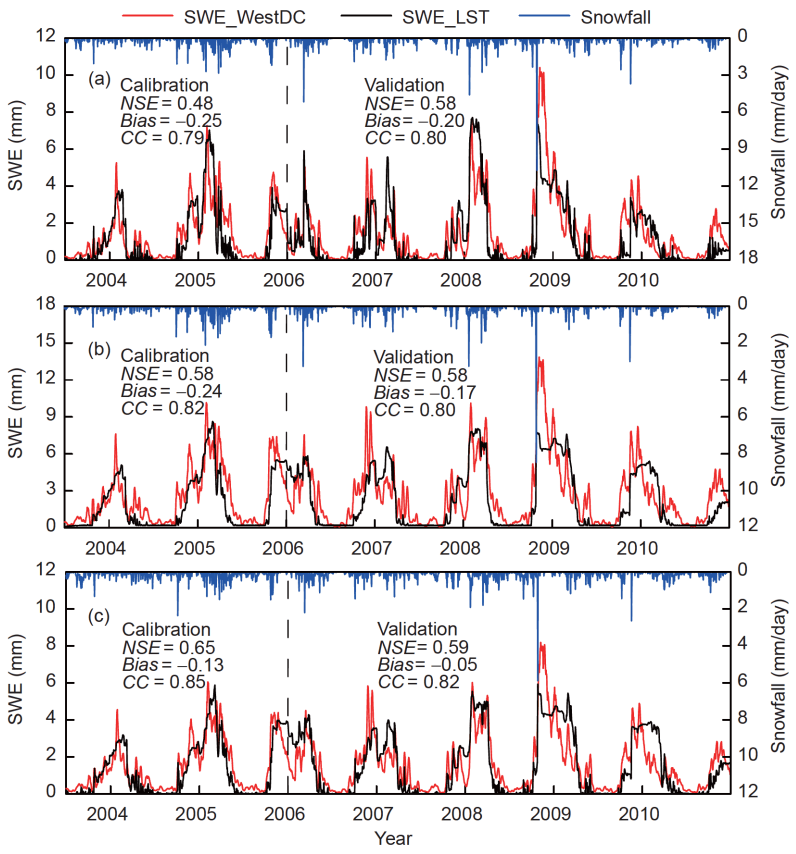

Figure 5 Daily PMW-based SWE time series (red line), simulated SWE time series (black line), and simulated snowfall time series driven by GSMaP and LST (blue solid bars) for the period Jul 2003–Dec 2010. Subplots (a)–(c) represent the Changdu, ULR, and LR basins, respectively.

simulated snowfall time series are shown in Figure 5. SWE simulations could not capture peaks of the SWE reference well, particularly in 2009 in all the three basins. This could be attributed to the overestimation of remotely sensed snow depths at the early stage of snow accumulation, because PMW-based snow depth retrievals are susceptible to the lower temperature of frozen soil in the TP [78]. The reference SWE is also subject to uncertainties due to the assumption of constant snow density over the season. The simulated SWE can be improved if snow redistribution and subcanopy melt processes are incorporated [79].

4.2 Snowmelt runoff modeling

GSMaP and LST were used as inputs of the CREST-snow model due to their good performance in SWE modeling as shown in Section 4.1. The CREST-snow model was used to simulate snowmelt runoff and total basin discharge in the ULR and LR basins, respectively. The simulated discharges for the two study basins could capture both peaks of the observations in summer and the streamflow during the low-flow period with *CC* values ranging from 0.85–0.92 and *NSE* values ranging from 0.62–0.80 during the overall study period (Figure 6). In the LR basin, the variation in discharge measurements and the peak flow have been gradually dampened during 2008–2011 due to operations of four seasonal regulation reservoirs (i.e., Gongguoqiao, Manwan, Dachaoshan, and Jinghong hydropower stations) on the LR. Both multi-year regulation reservoirs, i.e., the Xiaowan and Nuozhadu reservoirs on the LR started to operate after 2012, affecting the natural flow regime so greatly that the streamflow observations of the LR at the Yunjinghong gauging station has lost the seasonality (Figure 6(b)).

The proportion of snowmelt runoff to total runoff was found to be ~4% for the ULR during Jul 2011–Dec 2015 and also ~4% for the LR during Jan 2004–Dec 2014 (Table 3). Results obtained in the current and previous studies [33,50] suggest that the CREST-snow model is suited to simulate daily river discharge with *NSE* values more than 0.5. Overall, the proportion of snowmelt runoff to total runoff is relatively low in either the ULR or the LR basin. The impact of glacier meltwater on runoff is extremely limited with a contribution of no more than ~2% due to the limited glacierized area within the study basin.

4.3 Sensitivity analysis of snowmelt runoff modeling

Sensitivity analysis of parameters associated with snowmelt

Table 3 Contributions of different runoff components to total runoff (river discharge) in the ULR basin during Jul 2011–Dec 2015 and the Lancang River Basin during Jan 2004–Dec 2014

Basin	Rainfall	Snowmelt	Glacier melt
ULR	94.8%	4.1%	1.1%
LR	95%	4.3%	0.7%

runoff modeling was done in the ULR basin as an example to identify the effect of parameters on snowmelt and river discharge modeling during the overall study period of Jul 2011–Dec 2015. As shown in Figure 7(a), rainfall and snowfall temperature thresholds used to distinguish precipitation phase significantly affect the simulation of snowpack and the snowmelt process in the ULR basin. As the rainfall and snowfall temperature thresholds increase, both simulated snowfall and snowmelt runoff increase. However the total river discharge gradually decreases, implying that rainfall is the main factor of runoff generation in the ULR basin. The snowmelt contribution under the extreme situation (e.g., all the precipitation was considered as snow) was ~98% but not 100%, because the ratio of glacier meltwater to total river discharge accounted for ~2%. Both snowfall and snowmelt are controlled primarily by the rainfall and snowfall temperature thresholds in snow modeling based on the temperature index, and it is consistent with the conclusion of some previous studies [50,80].

Effect of the snowmelt temperature threshold on snowmelt runoff contribution is inconspicuous (Figure 7(b)). With decreasing snowmelt temperature threshold, snowmelt runoff contribution to total runoff increased from 0% to 3.7%. Snowfall in the ULR basin did not melt thoroughly when the snowmelt temperature threshold calibrated with remotely sensed SWE was −2.3°C. Figure 7(c) shows that the impact of degree-day factors on snowmelt runoff contribution is minimal with the contribution of snowmelt runoff varying within 0.5% as the parameters are changed. In addition, all the parameters associated with the snowmelt module have little impact on metrics of total runoff simulation which is

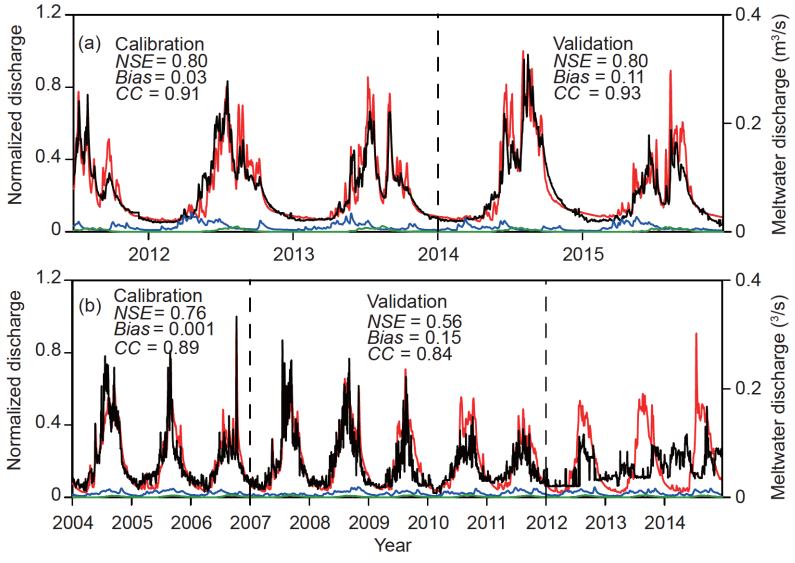

Figure 6 (a) Daily river discharge time series: simulated total river discharge (red line), observed total river discharge (black line), simulated snowmelt discharge (blue line) and simulated glacier meltwater (green line) at the Liutongjiang gauging station in the ULR basin from Jul 2011–Dec 2015; (b) the same for (a) but at the Yunjinghong gauging station in the LR basin from Jan 2004–Dec 2014.

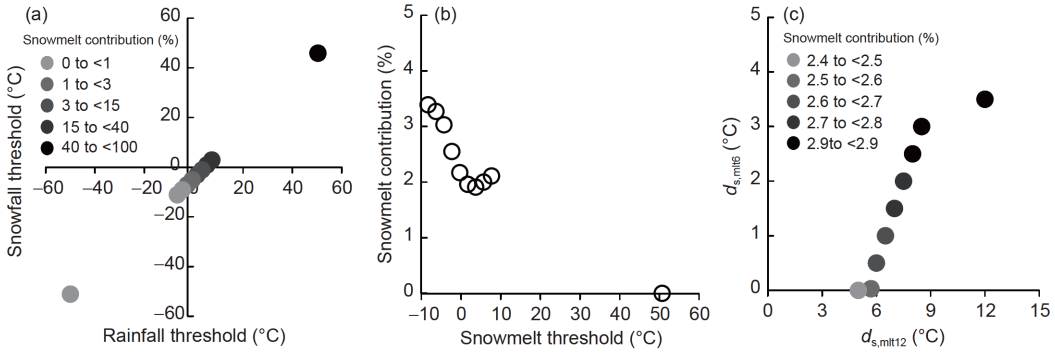

Figure 7 Effects of snow-related parameters including (a) rainfall and snowfall temperature thresholds, (b) snowmelt temperature threshold, and (c) degree-day factors on snowmelt runoff contributions in the ULR basin.

mainly due to the lower contribution of snowmelt to total discharge.

4.4 Evaluation of snowfall and snowmelt runoff modeling

Since the discrimination of the precipitation phase is the most important step in snowmelt modeling, we evaluated snowfall and snowmelt runoff modeling using snowfall observations from CMA. Figure 8 shows scatterplots of daily mean snowfall simulations using the CREST-snow model and daily mean snowfall observations from CMA at station Nos. 56018, 56125, and 56137 for the Jul 2003–Dec 2010 period. A statistical summary of metrics for snowfall modeling at the daily scale is shown in Table 4. Rajagopal and Harpold [81], and Zhong et al. [82] showed that the change of *CC* in snowfall modeling is very sensitive particularly in high-mountain regions. Moreover, Liu et al. [83] concluded that *CC* at the daily time step was lower than that at the annual time step. Therefore, the identification of snowfall is considered acceptable here when *CC*>0.20 at the daily time step. The CSI gives the overall fraction of correctly reflected snowfall events by modeling, which can be expressed as a function of POD and FAR [84]. When the two indices are consistent with the given criteria (CSI>0.2 and *CC*>0.2), the temperature thresholds can reasonably discriminate snowfall at these stations. The snowfall modeling is acceptable in terms of both timing and magnitude, with *CC* of 0.46, *Bias* of 8%, POD of 0.46, FAR of 0.54, and CSI of 0.29 on average. Bias values of snowfall modeling over Colorado from Rasmussen et al. [85] and Ikeda et al. [86] are higher than 10%, and the *CC* value of snowfall modeling from Liu et al. [83] is 0.2 in the Songhua River basin dominated by plains in Northeastern China. The well modeled snowfall here indicates the reliability of the rainfall and snowfall temperature thresholds derived from our snow hydrological model.

Next, rainfall and snowfall temperature thresholds derived from our model were compared with those derived from gauge observations that cannot, however, capture the detailed spatiotemporal variability of temperatures across mountainous terrain (Table 5). As mentioned in Section 3.1.4, the rainfall and snowfall temperature thresholds of a basin based on gauge observations were approximated by the mean of the thresholds of all rainfall gauges located within and surrounding the basin. There was almost no snow in the lower LR basin, so rainfall and snowfall temperature thresholds for the LR basin based on gauge observations was not calculated here. In the Changdu and ULR basins, rainfall and snowfall temperature thresholds derived from gauge observations was 5°C higher than that from the snow hydrological model. As shown in Figure 9, observed T_a time series is 5°C higher than the mean of LST and T_a time series in both the Changdu and ULR basins. This indicates that the observations cannot capture the detailed spatiotemporal variability of temperatures across mountainous terrain. If rainfall and snowfall temperature thresholds derived from gauge observations were used, it would lead to the overestimation of snowmelt runoff (Figure 7(a)).

Third, we compared percentages of total runoff originating as snowmelt and precipitation falling as snow in the two study basins. The LR basin was found to be of marked seasonal snow cover using snow cover observations from more than 700 meteorological stations in China for the 1960–2004 period [87]. Since there is less permanent snow in the LR basin, snowfall ratio and snowmelt contribution would be close in magnitude for a long time period without con-

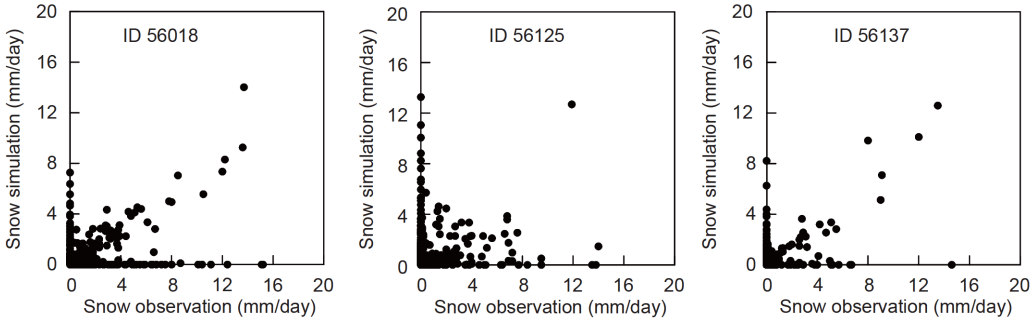

Figure 8 Scatterplots of daily mean snowfall simulations and observations at station Nos. 56018, 56125, and 56137 for the Jul 2003–Dec 2010 period.

Table 4 Statistical metrics of daily snowfall simulations at station Nos. 56018, 56125, and 56137 for the Jul 2003–Dec 2010 period

Station	*CC*	*RMSE*	*Bias*	POD	FAR	CSI
56018	0.42	1.2	−0.42	0.46	0.46	0.32
56125	0.34	0.99	0.28	0.53	0.63	0.28
56137	0.61	0.55	−0.11	0.4	0.53	0.28
Mean value	0.46	0.91	−0.08	0.46	0.54	0.29

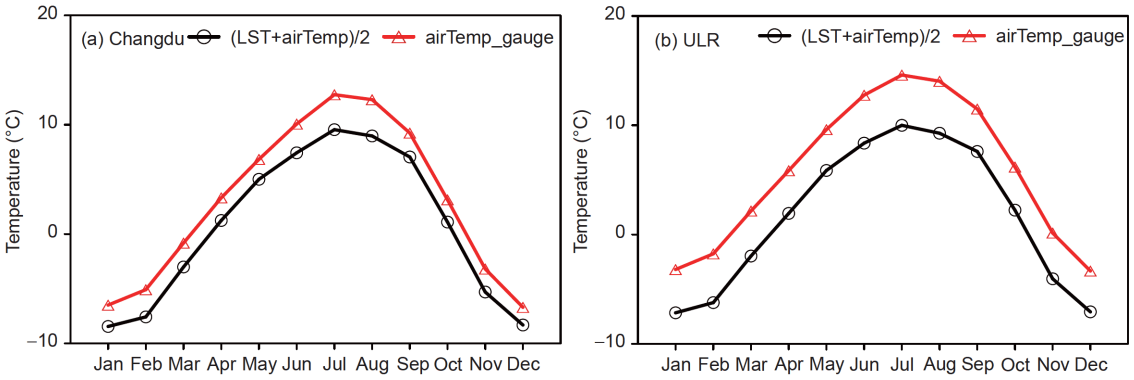

Figure 9 (Color online) Mean monthly arithmetic mean of LST and T_a, and mean monthly T_a from gauge observations for the Jul 2003–Dec 2010 period in the (a) Changdu and (b) ULR basin.

Table 5 Rainfall and snowfall thresholds based on the CREST-snow model and gauge observations

Basin	CREST-snow model		Rain gauge	
	T_r (°C)	T_s (°C)	T_r (°C)	T_s (°C)
Changdu	1.15	−2.25	7.78	1.98
ULR	−0.61	−3.62	5.28	1.44
LR	2.50	−0.32	–	–

sidering the time lag between snowfall and snowmelt. Here the observed snowfall was taken as an independent reference to evaluate the contributions of snowmelt runoff to total runoff. Results show that the snowfall ratio of 3.1% from the gauge observations is highly consistent with the proportional contribution of snowmelt runoff of 3.7% for the Jan 2004–Dec 2010 period in the LR basin (with mean annual rainfall of ~700 mm).

5 Discussion

Some studies evaluated Versions 6 and 7 of the Tropic Rainfall Measurement Mission (TRMM 3B42V7 and 3B42V6), and Version 4 Global Precipitation Measurement (GPM) mission Level 3 Integrated Multi-satellite Retrievals for GPM (IMERG) using gauge precipitation observations and applied them in river discharge modeling in the MRB [88,89]. Results show that remote sensing precipitation products are valuable in runoff modeling in the MRB. Our study shows the applicability of GSMaP in the LR basin. We found that GSMaP performs better than the rain gauge-based product in the study basins in terms of higher *NSE* values for SWE modeling. This manifests the potential of GSMaP precipitation estimates over ungauged or poorly gauged basins.

LST is a key variable in land-atmosphere interactions. Remotely sensed LST has often been used in deriving near-surface air temperature and it is commonly assumed that LST and T_a are strongly correlated particularly on clear-sky days [90,91]. Air temperature observations from meteorological stations provide limited information on spatial patterns over large areas. Joint use of LST and T_a in this study can provide tremendously valuable information at a spatial resolution of 1 km in the LR basin, better reflecting rain-snow partitioning and resulting in SWE simulations. They have also been implemented in other study areas such as the Yarlung Zangbo River basin and the Yangtze River basin [33,50].

Given the large impact of precipitation phase on snow modeling in our study areas, it is essential that model accurately partitions rain and snow using appropriate rainfall and snowfall temperature thresholds. Ding et al. [32] studied the dependence of precipitation phase on surface elevation using Daily Surface Climate Variables of China during 1951–1979 Version 3.0. They concluded that precipitation tends to fall as snow at high elevations and a higher temperature threshold is therefore needed for discriminating snowfall and rainfall. Jennings et al. [92] analyzed a 29-year observational data set, proposed a scheme for calculating rainfall and snowfall thresholds, and presented the first continuous Northern Hemisphere map of rain-snow thresholds. The rain-snow threshold over the TP in both studies was larger than 0°C. However, the best-fitted values of rainfall and snowfall temperature thresholds in our study basins were much lower than those in the two studies. Weather stations are generally located at lower or mid elevations. While these stations provide plenty of measurements, various studies have questioned the representativeness of such point-based measurements in alpine regions [93–95]. Therefore, determination of the rainfall and snowfall temperature thresholds of study basins can be very tricky, which cannot be completely dependent on point-based *in situ* measurements.

6 Conclusions

This study focuses on modeling of precipitation phase and

snow in the Changdu, ULR and LR basins in Southwest China. Major findings are summarized as follows.

(1) Compared with CGDPA, GSMaP performs better in SWE modeling with *NSE* values of 0.58, 0.58 and 0.59 for the Changdu, ULR and LR basins, respectively. This manifests the potential of GSMaP satellite precipitation over ungauged or poorly gauged basins. Joint use of high-resolution LST and air temperature products can more precisely distinguish precipitation phase than air and wet-bulb temperature products in the LR basin.

(2) Snowmelt runoff contributes ~4% to the total runoff of the ULR basin during Jul 2011–Dec 2015 and ~4% to the total runoff of the LR during Jan 2004–Dec 2014. The snowmelt runoff contributions agree with the snowfall proportion derived from the rain gauge data. Glacier meltwater is negligible, with contributions of no more than ~2%.

(3) Rainfall and snowfall temperature thresholds used to distinguish precipitation phase significantly affect snow modeling in temperature-index snow models. The rainfall and snowfall temperature thresholds derived from gauge observations are 5°C higher than those derived from the snow hydrological model through calibration with remotely sensed SWE in our study areas. Use of temperature thresholds derived from gauge observations would therefore lead to the overestimation of snowmelt runoff, because gauge observations cannot capture the detailed spatiotemporal variability of temperatures across mountainous terrain.

This study can serve as a basis for modeling and predicting snowmelt runoff in high-mountain regions and providing important reference to policy makers and water managers for the LR basin and its lower reaches in Southeast Asia.

This work was supported by the National Natural Science Foundation of China (Grant Nos. 51722903, 92047301, 51639005 and 91547210), and the National Key Research and Development Program of China (Grant No. 2018YFE0196000).

1 Parry M L, Canziani O F, Palutikof J P, et al. IPCC, 2007: Climate Change 2007: Impacts, Adaptation and Vulnerability. Contribution of Working Group II to the Fourth Assessment Report of the Intergovernmental Panel on Climate Change. Cambridge: Cambridge University Press, 2007
2 Immerzeel W W, Droogers P, de Jong S M, et al. Large-scale monitoring of snow cover and runoff simulation in Himalayan river basins using remote sensing. Remote Sens Environ, 2009, 113: 40–49
3 Jeelani G, Feddema J J, van der Veen C J, et al. Role of snow and glacier melt in controlling river hydrology in Liddar watershed (western Himalaya) under current and future climate. Water Resour Res, 2012, 48: e2011WR011590
4 Immerzeel W W, van Beek L P H, Bierkens M F P. Climate change will affect the Asian water towers. Science, 2010, 328: 1382–1385
5 Thompson J R, Green A J, Kingston D G. Potential evapotranspiration-related uncertainty in climate change impacts on river flow: An assessment for the Mekong River basin. J Hydrol, 2014, 510: 259–279
6 Hoang L P, Lauri H, Kummu M, et al. Mekong River flow and hydrological extremes under climate change. Hydrol Earth Syst Sci, 2016, 20: 3027–3041
7 Wang W, Lu H, Yang D, et al. Modelling hydrologic processes in the Mekong River Basin using a distributed model driven by satellite precipitation and rain gauge observations. PLoS ONE, 2016, 11: e0152229
8 Hoanh C T, Guttman H, Droogers P, et al. Water, climate, food, and environment in the Mekong basin in southeast Asia: Contribution to the project ADAPT: Adaptation strategies to changing environments. Final report. Colombo: International Water Management Institute, 2003
9 Lutz A F, Immerzeel W W, Shrestha A B, et al. Consistent increase in High Asia's runoff due to increasing glacier melt and precipitation. Nat Clim Change, 2014, 4: 587–592
10 Su F, Zhang L, Ou T, et al. Hydrological response to future climate changes for the major upstream river basins in the Tibetan Plateau. glob Planet Change, 2016, 136: 82–95
11 Moradkhani H, Hsu K L, Gupta H, et al. Uncertainty assessment of hydrologic model states and parameters: Sequential data assimilation using the particle filter. Water Resour Res, 2005, 41: e2004WR003604
12 Parajka J, Blöschl G. Spatio-temporal combination of MODIS images: Potential for snow cover mapping. Water Resour Res, 2008, 44: W03406
13 Famiglietti J S, Cazenave A, Eicker A, et al. Satellites provide the big picture. Science, 2015, 349: 684–685
14 Huang Q, Li X D, Han P F, et al. Validation and application of water levels derived from Sentinel-3A for the Brahmaputra River. Sci China Tech Sci, 2019, 62: 1760–1772
15 Brandt W T, Bormann K J, Cannon F, et al. Quantifying the spatial variability of a snowstorm using differential airborne lidar. Water Resour Res, 2020, 56: e2019WR025331
16 Li X, Long D, Han Z, et al. Evapotranspiration estimation for tibetan plateau headwaters using conjoint terrestrial and atmospheric water balances and multisource remote sensing. Water Resour Res, 2019, 55: 8608–8630
17 Sun Z, Long D, Yang W, et al. Reconstruction of GRACE data on changes in total water storage over the global land surface and 60 basins. Water Resour Res, 2020, 56: e26250
18 Huang Q, Long D, Du M, et al. Daily continuous river discharge estimation for ungauged basins using a hydrologic model calibrated by satellite altimetry: Implications for the SWOT mission. Water Resour Res, 2020, 56: e27309
19 Li X, Long D, Huang Q, et al. High-temporal-resolution water level and storage change data sets for lakes on the Tibetan Plateau during 2000–2017 using multiple altimetric missions and Landsat-derived lake shoreline positions. Earth Syst Sci Data, 2019, 11: 1603–1627
20 Abushandi E, Merkel B. Modelling rainfall runoff relations using HEC-HMS and IHACRES for a single rain event in an arid region of Jordan. Water Resour Manage, 2013, 27: 2391–2409
21 Yoshimoto S, Amarnath G. Applications of satellite-based rainfall estimates in flood inundation modeling—A case study in Mundeni Aru River Basin, Sri Lanka. Remote Sens, 2017, 9: 998
22 Bui H T, Ishidaira H, Shaowei N. Evaluation of the use of global satellite–gauge and satellite-only precipitation products in stream flow simulations. Appl Water Sci, 2019, 9: 53
23 Hock R. Temperature index melt modelling in mountain areas. J Hydrol, 2003, 282: 104–115
24 Harpold A A, Kaplan M L, Zion Klos P, et al. Rain or snow: Hydrologic processes, observations, prediction, and research needs. Hydrol Earth Syst Sci, 2017, 21: 1–22
25 Tang G, Wen Y, Gao J, et al. Similarities and differences between three coexisting spaceborne radars in global rainfall and snowfall estimation. Water Resour Res, 2017, 53: 3835–3853
26 Kulie M S, Milani L, Wood N B, et al. A shallow cumuliform snowfall census using spaceborne radar. J Hydrometeorol, 2016, 17: 1261–1279
27 Martinec J, Rango A, Major E. The Snowmelt-Runoff Model (SRM) User's Manual. 1983
28 Mitchell K. The community Noah land-surface model (LSM). User's Guide. ftp://ftp.emc.ncep.noaa.gov/mmb/gcp/ldas/noahlsm/ver_2

29 Bergström S. The HBV model: Its structure and applications. Report. Norrköping: Swedish Meteorological and Hydrological Institute, 1992
30 Anderson E. Snow accumulation and ablation model–SNOW-17. Report. Maryland: National Weather Service River Forecast System, 2006
31 Marks D, Winstral A, Reba M, et al. An evaluation of methods for determining during-storm precipitation phase and the rain/snow transition elevation at the surface in a mountain basin. Adv Water Resources, 2013, 55: 98–110
32 Ding B, Yang K, Qin J, et al. The dependence of precipitation types on surface elevation and meteorological conditions and its parameterization. J Hydrol, 2014, 513: 154–163
33 Chen X, Long D, Hong Y, et al. Improved modeling of snow and glacier melting by a progressive two-stage calibration strategy with GRACE and multisource data: How snow and glacier meltwater contributes to the runoff of the Upper Brahmaputra River basin? Water Resour Res, 2017, 53: 2431–2466
34 Gupta H V, Sorooshian S, Yapo P O. Toward improved calibration of hydrologic models: Multiple and noncommensurable measures of information. Water Resour Res, 1998, 34: 751–763
35 Dembélé M, Hrachowitz M, Savenije H H G, et al. Improving the predictive skill of a distributed hydrological model by calibration on spatial patterns with multiple satellite data sets. Water Resour Res, 2020, 56: e26085
36 Tekeli A E, Akyürek Z, Arda Şorman A, et al. Using MODIS snow cover maps in modeling snowmelt runoff process in the eastern part of Turkey. Remote Sens Environ, 2005, 97: 216–230
37 Steele C, Dialesandro J, James D, et al. Evaluating MODIS snow products for modelling snowmelt runoff: Case study of the Rio Grande headwaters. Int J Appl Earth Observation GeoInf, 2017, 63: 234–243
38 Wang J, Li H, Hao X. Responses of snowmelt runoff to climatic change in an inland river basin, Northwestern China, over the past 50 years. Hydrol Earth Syst Sci, 2010, 14: 1979–1987
39 Johnson M T, Ramage J, Troy T J, et al. Snowmelt detection with calibrated, enhanced-resolution brightness temperatures (CETB) in colorado watersheds. Water Resour Res, 2020, 56: e24542
40 Debeer C M, Pomeroy J W. Simulation of the snowmelt runoff contributing area in a small alpine basin. Hydrol Earth Syst Sci, 2010, 14: 1205–1219
41 Stigter E E, Wanders N, Saloranta T M, et al. Assimilation of snow cover and snow depth into a snow model to estimate snow water equivalent and snowmelt runoff in a Himalayan catchment. Cryosphere, 2017, 11: 1647–1664
42 Wang J, Hong Y, Li L, et al. The coupled routing and excess storage (CREST) distributed hydrological model. Hydrol Sci J, 2011, 56: 84–98
43 Du M, Long D. Development of a Hydrological Model Driven and Calibrated by Multisource Remote Sensing Data in Poorly Gauged Basins. Beijing: Tsinghua University, 2018. 1–61
44 Han Z, Long D, Huang Q, et al. Improving reservoir outflow estimation for ungauged basins using satellite observations and a hydrological model. Water Resour Res, 2020, 56: e27590
45 Shen Y, Xiong A. Validation and comparison of a new gauge-based precipitation analysis over mainland China. Int J Climatol, 2016, 36: 252–265
46 Jacobs J W. The Mekong River Commission: Transboundary water resources planning and regional security. Geographical J, 2002, 168: 354–364
47 Zhang L, Su F, Yang D, et al. Discharge regime and simulation for the upstream of major rivers over Tibetan Plateau. J Geophys Res Atmos, 2013, 118: 8500–8518
48 Samaniego L, Kumar R, Attinger S. Multiscale parameter regionalization of a grid-based hydrologic model at the mesoscale. Water Resour Res, 2010, 46: W05523
49 Larsen M A D, Refsgaard J C, Jensen K H, et al. Calibration of a distributed hydrology and land surface model using energy flux measurements. Agric For Meteor, 2016, 217: 74–88
50 Han P, Long D, Han Z, et al. Improved understanding of snowmelt runoff from the headwaters of China's Yangtze River using remotely sensed snow products and hydrological modeling. Remote Sens Environ, 2019, 224: 44–59
51 Liu J, Zhang W, Xia J, et al. Study of degree-day model from 2000 to 2016: The main processes and key issues. J Glaciol Geocryol, 2017, 39: 801–810
52 Van Tiel M, Teuling A J, Wanders N, et al. The role of glacier changes and threshold definition in the characterisation of future streamflow droughts in glacierised catchments. Hydrol Earth Syst Sci, 2018, 22: 463–485
53 Engelhardt M, Schuler T V, Andreassen L M. Contribution of snow and glacier melt to discharge for highly glacierised catchments in Norway. Hydrol Earth Syst Sci, 2014, 18: 511–523
54 Zhao R J. The Xinanjiang model applied in China. J Hydrol, 1992, 135: 371–381
55 Shen X, Hong Y, Zhang K, et al. Refining a distributed linear reservoir routing method to improve performance of the CREST model. J Hydrol Eng, 2016, 22: 04016061
56 Deb K, Pratap A, Agarwal S, et al. A fast and elitist multiobjective genetic algorithm: NSGA-II. IEEE Trans Evol Computat, 2002, 6: 182–197
57 Kayastha R B, Steiner N, Kayastha R, et al. Comparative study of hydrology and icemelt in three nepal river basins using the glacio-hydrological degree-day model (GDM) and observations from the advanced scatterometer (ASCAT). Front Earth Sci, 2020, 7: 354
58 Han Z, Long D, Fang Y, et al. Impacts of climate change and human activities on the flow regime of the dammed Lancang River in Southwest China. J Hydrol, 2019, 570: 96–105
59 Li B, Su H, Chen F, et al. The changing pattern of droughts in the Lancang River Basin during 1960–2005. Theor Appl Climatol, 2013, 111: 401–415
60 Tang G, Zeng Z, Long D, et al. Statistical and hydrological comparisons between TRMM and GPM level-3 products over a midlatitude basin: Is day-1 IMERG a good successor for TMPA 3B42V7? J Hydrometeorol, 2016, 17: 121–137
61 Xie P, Yatagai A, Chen M, et al. A gauge-based analysis of daily precipitation over East Asia. J Hydrometeorol, 2007, 8: 607–626
62 Ushio T, Sasashige K, Kubota T, et al. A Kalman filter approach to the Global Satellite Mapping of Precipitation (GSMaP) from combined passive microwave and infrared radiometric data. J Meteor Soc Japan, 2009, 87A: 137–151
63 Bao X, Zhang F. Evaluation of NCEP-CFSR, NCEP-NCAR, ERA-Interim, and ERA-40 reanalysis datasets against independent sounding observations over the Tibetan Plateau. J Clim, 2013, 26: 206–214
64 Bai L, Long D, Yan L. Estimation of surface soil moisture with downscaled land surface temperatures using a data fusion approach for heterogeneous agricultural land. Water Resour Res, 2019, 55: 1105–1128
65 Long D, Yan L, Bai L, et al. Generation of MODIS-like land surface temperatures under all-weather conditions based on a data fusion approach. Remote Sens Environ, 2020, 246: 111863
66 Zeng C, Shen H, Zhong M, et al. Reconstructing MODIS LST based on multitemporal classification and robust regression. IEEE Geosci Remote Sens Lett, 2015, 12: 512–516
67 Duan S B, Li Z L, Wang N, et al. Evaluation of six land-surface diurnal temperature cycle models using clear-sky *in situ* and satellite data. Remote Sens Environ, 2012, 124: 15–25
68 Schädlich S, Göttsche F M, Olesen F S. Influence of land surface parameters and atmosphere on METEOSAT brightness temperatures and generation of land surface temperature maps by temporally and spatially interpolating atmospheric correction. Remote Sens Environ, 2001, 75: 39–46
69 Yang J, Jiang L, Ménard C B, et al. Evaluation of snow products over the Tibetan Plateau. Hydrol Process, 2015, 29: 3247–3260
70 Che T, Xin L, Jin R, et al. Snow depth derived from passive microwave remote-sensing data in China. Ann Glaciol, 2008, 49: 145–154

71 Dai L, Che T, Ding Y. Inter-calibrating SMMR, SSM/I and SSMI/S data to improve the consistency of snow-depth products in China. Remote Sens, 2015, 7: 7212–7230
72 Dai L, Che T, Wang J, et al. Snow depth and snow water equivalent estimation from AMSR-E data based on a priori snow characteristics in Xinjiang, China. Remote Sens Environ, 2012, 127: 14–29
73 Dai L, Che T, Xie H, et al. Estimation of snow depth over the Qinghai-Tibetan Plateau based on AMSR-E and MODIS data. Remote Sens, 2018, 10: 1989
74 Verdin J, Funk C, Senay G, et al. Climate science and famine early warning. Phil Trans R Soc B, 2005, 360: 2155–2168
75 Kiem A S, Ishidaira H, Hapuarachchi H P, et al. Future hydroclimatology of the Mekong River basin simulated using the high-resolution Japan Meteorological Agency (JMA) AGCM. Hydrol Process, 2008, 22: 1382–1394
76 Moriasi D N, Arnold J G, Van Liew M W, et al. Model evaluation guidelines for systematic quantification of accuracy in watershed simulations. Trans ASABE, 2007, 50: 885–900
77 Harder P, Pomeroy J. Estimating precipitation phase using a psychrometric energy balance method. Hydrol Process, 2013, 27: 1901–1914
78 Dai L, Che T, Ding Y, et al. Evaluation of snow cover and snow depth on the Qinghai–Tibetan Plateau derived from passive microwave remote sensing. Cryosphere, 2017, 11: 1933–1948
79 Lv Z, Pomeroy J W, Fang X. Evaluation of SNODAS snow water equivalent in Western Canada and assimilation into a cold region hydrological model. Water Resour Res, 2019, 55: 11166–11187
80 Alder J R, Hostetler S W. The dependence of hydroclimate projections in snow-dominated regions of the Western United States on the choice of statistically downscaled climate data. Water Resour Res, 2019, 55: 2279–2300
81 Rajagopal S, Harpold A A. Testing and improving temperature thresholds for snow and rain prediction in the Western United States. J Am Water Resour Assoc, 2016, 52: 1142–1154
82 Zhong K, Zheng F, Xu X, et al. Discriminating the precipitation phase based on different temperature thresholds in the Songhua River Basin, China. Atmos Res, 2018, 205: 48–59
83 Liu S, Yan D, Qin T, et al. Precipitation phase separation schemes in the Naqu River basin, eastern Tibetan plateau. Theor Appl Climatol, 2018, 131: 399–411
84 Tang G, Ma Y, Long D, et al. Evaluation of GPM Day-1 IMERG and TMPA Version-7 legacy products over Mainland China at multiple spatiotemporal scales. J Hydrol, 2016, 533: 152–167
85 Rasmussen R, Liu C, Ikeda K, et al. High-resolution coupled climate runoff simulations of seasonal snowfall over Colorado: A process study of current and warmer climate. J Clim, 2011, 24: 3015–3048
86 Ikeda K, Rasmussen R, Liu C, et al. Simulation of seasonal snowfall over Colorado. Atmos Res, 2010, 97: 462–477
87 Wang C, Wang Z, Cui Y. Snow cover of China during the last 40 years: Spatial distribution and interannual variation. J Glaciol Geocryol, 2009, 31: 301–310
88 Zeng H, Li L, Li J. The evaluation of TRMM Multisatellite Precipitation Analysis (TMPA) in drought monitoring in the Lancang River Basin. J Geogr Sci, 2012, 22: 273–282
89 He Z, Yang L, Tian F, et al. Intercomparisons of rainfall estimates from TRMM and GPM multisatellite products over the Upper Mekong River Basin. J Hydrometeorol, 2017, 18: 413–430
90 Benali A, Carvalho A C, Nunes J P, et al. Estimating air surface temperature in Portugal using MODIS LST data. Remote Sens Environ, 2012, 124: 108–121
91 Colombi A, De Michele C, Pepe M, et al. Estimation of daily mean air temperature from MODIS LST in Alpine areas. EARSeL eProceedings, 2007, 6: 38–46
92 Jennings K S, Winchell T S, Livneh B, et al. Spatial variation of the rain-snow temperature threshold across the Northern Hemisphere. Nat Commun, 2018, 9: 1148
93 Helbig N, van Herwijnen A. Subgrid parameterization for snow depth over mountainous terrain from flat field snow depth. Water Resour Res, 2017, 53: 1444–1456
94 Shen Y J, Shen Y, Fink M, et al. Unraveling the hydrology of the glacierized Kaidu Basin by integrating multisource data in the Tianshan Mountains, Northwestern China. Water Resour Res, 2018, 54: 557–580
95 Huning L S, Margulis S A. Climatology of seasonal snowfall accumulation across the Sierra Nevada (USA): Accumulation rates, distributions, and variability. Water Resour Res, 2017, 53: 6033–6049